

CLOSED-FORM ASYMPTOTICS FOR LOCAL VOLATILITY MODELS

WEN CHENG, NICK COSTANZINO, JOHN LIECHTY, ANNA MAZZUCATO,
AND VICTOR NISTOR

ABSTRACT. We obtain new closed-form pricing formulas for contingent claims when the asset follows a Dupire-type local volatility model. To obtain the formulas we use the Dyson-Taylor commutator method that we have recently developed in [5, 6, 8] for short-time asymptotic expansions of heat kernels, and obtain a family of general closed-form approximate solutions for both the pricing kernel and derivative price. A bootstrap scheme allows us to extend our method to large time. We also perform analytic as well as a numerical error analysis, and compare our results to other known methods.

CONTENTS

1. Introduction	1
2. Theoretical Framework	7
3. Closed Form Approximate Solutions	17
4. Comparison and Performance of the Method	18
5. Option pricing with long maturity: the bootstrap scheme	22
References	27

1. INTRODUCTION

Financial derivatives (also known as contingent claims) are now a ubiquitous tool in risk management with approximately 600 trillion dollars worth of such contracts currently in the market. The pricing of such derivatives is therefore an active area of research in both Mathematics and Finance (see for example [12, 15, 17, 21, 32] and the references therein). In this paper, we will apply the perturbative (asymptotic) method introduced in [8] for numerically solving parabolic equations and then use this method to price European options.

One of the earliest models used in pricing derivatives is the Black-Scholes-Merton model [3, 27], for which the movement in the price X_t of the underlying asset on which the claim is based is modeled by geometric Brownian

Date: October 30, 2018.

A.M. was partially supported by NSF Grant DMS 0708902. V.N. was partially supported by NSF grant DMS-0555831, DMS-0713743, and OCI 0749202.

motion. For the Black-Scholes-Merton as well as for other models given by stochastic differential equations, the pricing of European options can be reduced to the calculation of certain solutions of parabolic equations, obtained through Ito's Lemma (and the change of variables $t \leftarrow T - t$) in the backward Kolmogorov equation. The resulting equation is a Fokker-Planck equation, which is an equation of parabolic type. Fokker-Planck equations more generally have important applications in statistical mechanics and in probability (see for example the monographs [4, 16, 30]). Given that the asset price is always assumed positive, the Fokker-Planck equation is solved on the positive half-line. One difficulty in treating this type of the equation is that the coefficients of the Fokker-Planck operator typically vanish at the boundary, making the equation degenerate.

For example, for the Black-Scholes-Merton model, the resulting Fokker-Planck equation is given by

$$(1.1) \quad \begin{cases} \partial_t U(t, x) - LU(t, x) = 0, & 0 < t < T, x > 0 \\ U(0, x) = h(x), & x > 0, \end{cases}$$

where

$$(1.2) \quad L := \frac{1}{2}\sigma^2 x^2 \partial_x^2 + rx \partial_x - r,$$

is the *Black-Scholes operator*, a degenerate elliptic operator, t is the time to expiry, and h is the so-called *pay-off* function. For a *European Call option with strike K* and expiry (or exercise) date T , the pay-off function h is given by the formula $h(x_T) = |x_T - K|_+ := \max\{x_T - K, 0\}$, where x_T is the price of the underlying asset at time T . Above, σ and r are constant parameters, representing respectively the *volatility* of the underlying asset, and the current *interest rate*. Since the operator is degenerate at the boundary $x = 0$, it can be shown that the solution automatically vanishes there and no explicit boundary condition need to be imposed.

A popular model related to the Black-Scholes-Merton model is the CEV model [10]. In the CEV model, the operator L is the form

$$(1.3) \quad L(t, x) = L(x) = \frac{1}{2}\sigma^2 x^{2\alpha} \partial_x^2 + rx \partial_x - r,$$

where σ , α , r are constant. Yet another popular model is Dupire's local volatility model, for which we allow the volatility to change with time:

$$L(t, x) = L(x) = \frac{1}{2}\sigma^2(x, t)x^2 \partial_x^2 + rx \partial_x - r.$$

Except in special cases, such as the Black-Scholes-Merton equation above and when L has constant coefficients, very few exact solution formulas to the problem (1.1) are available. It is therefore important to devise fast, accurate approximate solution methods. The focus of this paper is on obtaining approximate solution methods that are fast and accurate by combining standard numerical methods with the asymptotic techniques developed in [8]. Fast solution methods are crucial when calibrating unknown parameters,

especially in the Bayesian inference framework. We hope to address this question in a forthcoming paper.

In view of the above discussion, it is justified to study the forward initial-value problem (1.1) for the general case when L is an operator of the form:

$$(1.4) \quad L(t) := \frac{1}{2}a(t, x)^2\partial_x^2 + b(t, x)\partial_x + c(t, x).$$

We therefore allow for *variable* coefficients *in both space and time*. We assume throughout that $a(x) > 0$, for $x > 0$ and that the coefficients a , b , c are smooth functions. The perturbative method introduced in [8] for the study of parabolic equations in arbitrary dimensions was fully justified in the case when a , b , and c and all their derivatives are bounded, and are bounded away from zero: $a(x) \geq \gamma > 0$. In this paper we complete the results of [8] with explicit formulas for the 1D case. Then we numerically test our formulas for the Black-Scholes-Merton and CEV models, obtaining an excellent agreement between our theoretical results and the numerical tests. Both the Black-Scholes-Merton model (1.2) and the CEV model (1.3) are more general than the models considered in [8] in that their coefficients do not satisfy the assumptions of the paper, yet the numerical tests indicate that the results of that paper are still valid for the more general models considered here. This observation suggests that the theoretical framework of [8] is applicable in greater generality. We plan to study this point in a forthcoming paper.

To explain our method, let us recall that, under certain conditions on the operator L and initial value h , described in details in the next section, there exists a *smooth function* $\mathcal{G}_t(x, y)$ such that the solution to (1.1) has the representation

$$(1.5) \quad U(t, x) = \int_0^\infty \mathcal{G}_t(x, y)h(y)dy.$$

The kernel function $\mathcal{G}_t(x, y)$ in (1.5) is the fundamental solution or the so-called *Green function* for the problem (1.1).

Remark 1.1. Given that $\mathcal{G}_t(x, y)$ arises in several different contexts, we will call the function $\mathcal{G}_t(x, y)$ the *transition density kernel*, *pricing kernel*, *heat kernel*, or *Green function* interchangeably, depending on the context in which the object arises.

As mentioned above, except for some very special cases no explicit formulas for $\mathcal{G}_t(x, y)$ or $U(t, x)$ are available. For the Black-Scholes-Merton model, a change of variables reduces the PDE to a heat equation that can then be solved explicitly. Therefore, exact formulas for the kernel \mathcal{G}^{BSM} and the

solution U^{BSM} exist, which we recall now for further reference:

$$(1.6) \quad \begin{aligned} \mathcal{G}_t^{BSM}(x, y) &= \frac{\exp(-rt)}{y\sqrt{2\pi\sigma^2t}} \exp\left(-\frac{|\ln(x/y) + (r - \sigma^2/2)t|^2}{2\sigma^2t}\right) \\ U^{BSM}(t, x) &= \int_0^\infty \mathcal{G}_t^{BSM}(x, y) dy = x\mathcal{N}(d_-) + Ke^{-rt}\mathcal{N}(d_+), \end{aligned}$$

where $\mathcal{N}(x) = \int_{-\infty}^x \frac{1}{\sqrt{2\pi}} e^{-z^2/2}$ is the cumulative normal distribution function (cumulative Gaussian distribution function) and

$$(1.7) \quad d_\pm = \frac{\ln(x/K) + (r \pm \sigma^2/2)t}{\sigma\sqrt{t}}.$$

However, for the time-dependent Black-Scholes-Merton model, where σ and r are time-dependent, or local volatility models in general, closed form solutions are generally given by series expansions and difficult to use in practice or are not known (see, for instance, [11, 23]).

The method that we use in this paper is to give an approximate closed-form solution for the equation (1.1) by giving an approximate closed-form expansion for the Green's function $\mathcal{G}_t(x, y)$. Since our approximation of the Green's function is in terms of Gaussian-type integrals, it gives a closed-form for the approximate price of a European call option for *any* one-dimensional model where the operator L is given by (1.4). In fact, as an application, we give the prices and Greeks (that is, suitable derivatives) of a European call option and perform an error analysis in Section 4.

There exists a vast literature on obtaining asymptotic expansions of the Green's function $\mathcal{G}_t(x, y)$ when t small and x is close to y , especially in the case that L is independent of time [2, 20, 22, 25, 28, 35, 35, 36]. (See also [1, 14, 18, 26, 34]). Many of these methods are based on a geometric interpretation of the operator L (or at least its principal part) as a Laplace operator on curved space, and require computing the geodesics in this space, which very often must be done numerically. Other approaches are based on pseudo-differential calculus. In particular, Corielli, Foschi, and Pascucci [7] use a *parametrix* construction for the problem (1.1) to obtain a closed-form approximate solution. We recently developed in [5, 6, 8] a complementary approach to computing short-time asymptotics for \mathcal{G}_t , based on parabolic rescaling, Taylor's expansions of the coefficients, Duhamel's and Dyson's formulas, and exact commutator expansion. We called this method the *Dyson-Taylor commutator method*. Our method is more elementary and appears very stable in practical implementations.

Let us fix a function $z = z(x, y)$ with the properties that $z(x, x) = x$ and all its derivatives are bounded. The function z will represent the *base-point* for a parabolic rescaling of the Green's function. Then our short-time

asymptotics give an expansion for the kernel in the form:

$$(1.8) \quad \begin{aligned} \mathcal{G}_t(x, y) &= \mathcal{G}_t^{[n]}(x, y; z) + t^{(n+1)/2} \mathcal{E}_t^{[n]}(x, y; z) \\ \mathcal{G}_t^{[n]}(x, y; z) &= G_t^{[0]}(x, y; z) + t^{1/2} G_t^{[1]}(x, y; z) + \cdots + t^{n/2} G_t^{[n]}(x, y; z), \end{aligned}$$

where $\mathcal{G}_t^{[n]}$ is the sum on the first n terms of the expansion and represents the n -th order approximate kernel, while $t^{(n+1)/2} \mathcal{E}_t^{[n]}$ is the remainder. The first term, $G_t^{[0]}$ is given by a dilated Gaussian function

$$(1.9) \quad G_t^{[0]}(x, y) = G_t^{[0]}(x - y) = \frac{1}{\sqrt{2t\pi a(0, z)^2}} \exp\left(-\frac{|x - y|^2}{2ta(0, z)^2}\right).$$

The Dyson-Taylor commutator method yields an explicit algorithm to compute the terms $G_t^{[n]}$ for *any* n , if L is an operator of the form (1.4) and corresponding analogs in higher dimension.

More precisely, our main result in [8] is that for the local volatility operator (1.4), the n -th order approximate kernel has the form

$$(1.10) \quad G_t^{[k]}(x, y) := t^{-1/2} \mathfrak{P}^k\left(z, z + \frac{x - z}{t^{1/2}}, \frac{x - y}{t^{1/2}}\right) G_t^{[0]}\left(\frac{x - y}{t^{1/2}}\right),$$

where the functions $\mathfrak{P}^\ell(z, x, y)$ are algorithmically computable (recall that $z = z(x, y)$). In this paper we shall compute the functions \mathfrak{P}^k , for $k = 0, 1, 2$ at an *arbitrary* basepoint z . The details, based on the Dyson-Taylor commutator method method, can be found in Section 2 and 2.1. We therefore obtain *new* closed form asymptotic expansions of the Green function for local volatility models. In particular, the first order asymptotic expansion at arbitrary $z = z(x, y)$ is given by

$$(1.11) \quad \begin{aligned} \mathcal{G}_t^{[1]}(x, y; z) &= \frac{1}{\sqrt{2\pi t a(0, z)^2}} \left[1 + \frac{3a(0, z)a'(0, z) - 2b(0, z)}{2a(0, z)^2} (x - y) \right. \\ &\quad \left. - \frac{a'(0, z)}{2t a(0, z)^3} (x - y)^3 + (x - z) \frac{(x - y)^2 - t a(0, z)^2}{t a(0, z)^3} \right] e^{-\frac{|x - y|^2}{2t a(0, z)^2}}. \end{aligned}$$

We provide an explicit formula for the second order expansion of the Green function at the end of Section 2. This algorithm can be implemented very efficiently at least in dimension 1 and for n small, $n = 1, n = 2$. The numerical tests in Section 4 show that already the second-order approximation is adequate for the Black-Scholes and CEV models.

For each term $G_t^{[k]}$ in the expansion of the Green function, let $\mathcal{U}^{[k]}$ denote the corresponding term in the expansion of the solution,

$$(1.12) \quad \mathcal{U}^{[k]}(t, x) = \int_0^\infty G_t^{[k]}(x, y) h(y; K) dy.$$

Then using (1.5) and (1.8), we arrive at the expansion of the value of the contingent claim,

$$(1.13) \quad \begin{aligned} U(t, x) &= U^{[n]}(t, x) + t^{(n+1)/2} \mathfrak{E}^{[n]}(t, x) \\ U^{[n]}(t, x) &= \mathcal{U}^{[0]}(t, x) + t^{1/2} \mathcal{U}^{[1]}(t, x) + t \mathcal{U}^{[2]}(t, x) + \dots + t^{n/2} \mathcal{U}^{[n]}(t, x) \end{aligned}$$

where

$$(1.14) \quad t^{(n+1)/2} \mathfrak{E}^{[n]}(t, x) := t^{(n+1)/2} \int_0^\infty \mathcal{E}_t^{[n]} h(y; K) = U(t, x) - U^{[n]}(t, x)$$

is the remainder term (or error) in the expansion of the solution. In [8] we have shown that the remainder can be controlled in exponentially weighted Sobolev norms, when the operator L is uniformly strongly elliptic. These bounds on the remainder imply that, in this case, the error made by replacing \mathcal{G}_t with $\mathcal{G}_t^{[n]}$ in (1.5) is of order $t^{n/2}$ *globally* in space, the expected optimal rate. In [5], we consider degenerate operators, the symbol of which is strongly elliptic with respect to some complete metric of bounded geometry. For example, the Black-Scholes and the SABR models fit into this framework. By contrast, the CEV model with $0 < \beta < 1$ does not fit into this framework. Our numerical tests indicate nevertheless that the error term has the same order in t even for the CEV model with $\beta < 1$. For pedagogical purposes and error analysis we will list all the details for the time-dependent Black-Scholes and CEV models, although our results are more general.

In Section 4 we perform a numerical error analysis by computing both the numerical solution U and expansion $U^{[n]}$ and estimating the error

$$(1.15) \quad |U(t, x) - U^{[n]}(t, x)|$$

pointwise for the basepoint $z(x, y) = x$, when $n = 1, 2$. The error analysis is in good agreement with the theoretical results, even though the local volatility operators considered in this paper do not necessarily satisfy the assumptions on the coefficients of L needed to establish the analytic error estimates performed in [5, 6, 8].

In Section 4 we then perform an error analysis. For the Black-Scholes-Merton model, for which an exact solution formula is readily available, we compare the expansions at the basepoint $z(x, y) = x$ with the exact solution. (Note however, that numerical errors arise also in the calculation of exact solutions, due to round-off errors and other approximations.) For the CEV model, we compare the expansions with benchmark formulas in the literature, in particular the Hagan-Woodward implied volatility approximation [19].

Given that the kernel approximation is asymptotic in time, it guarantees good error control *a priori* only for sufficiently small t . In Section 5, we shall introduce a bootstrap scheme to extend our method to arbitrary large time. This strategy is based on the evolutionary property of the solution operator to (1.1). By doing so, we show that the error is remarkably reduced. As an application in portfolio management, we also compute the Greeks (or

hedging parameters) of a European call option and compare our approximations with the true Black-Scholes Greeks in Section 4.2 and Section 5. These applications again underline the accuracy of our methods.

Acknowledgements. The authors would like to thank Marco Avellaneda for valuable suggestions and comments on the manuscript, and Jim Gatheral for useful discussions. Victor Nistor also gladly acknowledges support from the Max Planck Institute for Mathematics, where part of this work has been performed.

2. THEORETICAL FRAMEWORK

We begin by recalling the Dyson-Taylor commutator method, which we introduced in [6, 8], to obtain small-time asymptotic expansions for the solution of the initial-value problem:

$$(2.1) \quad \begin{aligned} \partial_t U(t, x) - L(t)U(t, x) &= 0 \\ U(0, x) &= h(x). \end{aligned}$$

Throughout the paper, the operator L will be given by (1.4), and we will omit the explicit dependence of L and of its coefficients on x . In addition, we tacitly assume that all the coefficients of L are regular enough to carry out the manipulations described next. For a rigorous justification in the case L is not degenerate, we refer to [6, 8].

If there is a unique solution to the initial-value problem (2.1), then the linear operator that maps the initial data h to the solution U is well defined. We refer to such operator as the *solution operator*. For constant-coefficient second-order operators, L_0 , the solution operator forms a *semigroup*, denoted by e^{tL_0} , $t > 0$; that is, the solution operator has the following properties:

- (i) $e^{tL_0}|_0 = I$.
- (ii) $e^{t_1L_0} e^{t_2L_0} = e^{(t_1+t_2)L_0}$, $t_1, t_2 > 0$.

The same conclusion hold for variable-coefficient, but time-independet operators L , under some conditions, for instance if L is strongly elliptic [29] (that is, $a(x) \geq \gamma > 0$ for all x). When L is a time-dependent operator, $L = L(t)$, the solution operator is no more a semigroup, but under some additional mild conditions, forms an *evolution system* $\mathcal{S}(t_1, t_2)$ [6, 24]. For an evolution system, property (2) is replaced by $\mathcal{S}(t_1, t_2)\mathcal{S}(t_2, t_3) = \mathcal{S}(t_1, t_3)$, if $0 \leq t_3 \leq t_2 \leq t_1$. Following the notation set forth in the Introduction, we denote the kernel or Green's function of the solution operator to the problem (2.1) by \mathcal{G}_t^L .

Our method relies heavily on the study of distribution kernels of the evolution operators defined by our Fokker-Planck operator, so a brief discussion of distribution kernels and of our conventions is in order.

Remark 2.1. Given a linear operator T mapping smooth functions with compact support into distributions, there exist a *distribution kernel* k_T

such that

$$(2.2) \quad Tu(x) = \int k_T(x, y) u(y) dy.$$

The integral above is interpreted as the pairing between test functions and distributions. In this paper, we will be interested in the integral representation (2.2) in the case that T is a *smoothing operator*, that is, an operator that maps compactly supported distributions into smooth functions. Then, the kernel k_T is a *smooth function*, and the notation $k_T(x, y)$ is justified point-wise. (For a more detailed discussion, see for example [33].) In this case, we will write $T(x, y)$ to denote the kernel $k_T(x, y)$, and in general, *we shall identify an operator with its distribution kernel*. Let f be a smooth function, then we denote the operators of multiplication by f also with f . Additionally, we notice that there is no confusion when writing fT or Tf since the distribution kernels of these operators are given by $fT(x, y) = f(x)T(x, y)$ or $Tf(x, y) = T(x, y)f(y)$. Similarly, there is no confusion when writing $\partial_x T(x, y)$, since the distribution kernel of $\partial_x T$ is $(\partial_x k_T)(x, y) = \partial_x(k_T(x, y))$. However $k_{T\partial_x}(x, y) = -\partial_y k_T(x, y)$.

We now introduce parabolic rescaling, which is a basic tool used in this paper. Let z be a fixed, but arbitrary point in \mathbb{R} and $s > 0$ a parameter. Given a function $f(t, x)$ we denote by

$$(2.3) \quad f^{s,z}(t, x) := f(s^2 t, z + s(x - z)),$$

the *parabolic rescaling by s of the function f about $(0, z)$* . Thus $h^{s,z}(x) := h(z + s(x - z))$ for a function that does not depend on t . We will refer to z as the *basepoint* for the rescaling. Similarly, we define a rescaled operator $L^{s,z}$ by

$$(2.4) \quad L^{s,z}(t, x) := \frac{1}{2} a^{s,z}(t, x)^2 \partial_x^2 + s b^{s,z}(t, x) \partial_x + s^2 c^{s,z}(t, x).$$

If U solves the initial-value problem (2.1), then $U^{s,z}$ solves the rescaled problem

$$(2.5) \quad \begin{aligned} \partial_t U^{s,z}(t, x) - L^{s,z}(t, x) U^{s,z}(t, x) &= 0 \\ U^{s,z}(0, x) &= h^{s,z}(x) \end{aligned}$$

Consequently, the Green functions of the operator $\partial_t - L$ and of the rescaled operator $\partial_t - L^{s,z}$ are related by

$$(2.6) \quad \begin{aligned} \mathcal{G}_t^L(x, y) &= s^{-1} \mathcal{G}_{s^{-2}t}^{L^{s,z}}(z + s^{-1}(x - z), z + s^{-1}(y - z)) \\ &= t^{-\frac{1}{2}} \mathcal{G}_1^{L^{\sqrt{t}, z}}(z + t^{-\frac{1}{2}}(x - z), z + t^{-\frac{1}{2}}(y - z)), \text{ if } s = t^{\frac{1}{2}}. \end{aligned}$$

We now proceed to compute the Green's function $G_t^{L^{s,z}}$ of the rescaled problem (2.5) when $t = 1$. In order to do so, we shall consider the Taylor expansion in s at $s = 0$ of the rescaled operator $L^{s,z}$, given in equation (2.4), up to order n . By ‘‘Taylor expansion’’ we mean that we Taylor expand the

coefficients of $L^{s,z}$ and group all terms of the same order in s . The operator $L^{s,z}$ can then be written as follows

$$(2.7) \quad L^{s,z} = \sum_{k=0}^n s^k L_k^z + s^{n+1} L_{n+1}^{s,z}(t, x),$$

where $L_{n+1}^{s,z}(t, x)$ contains all the remainder terms from the Taylor expansion of the coefficients.

In this paper, we concentrate on calculating explicitly the second-order approximation of the Green function of L . Hence, *we fix $n = 2$ from now on*. For notational convenience, we denote $g'(t, x) = \frac{\partial}{\partial x} g(t, x)$ and $\dot{g}(t, x) = \frac{\partial}{\partial t} g(t, x)$. Then the second-order Taylor expansion in s of $f^{s,z}$ at $s = 0$ is given by

$$(2.8) \quad f^{s,z}(t, x) = f(0, z) + s(x - z)f'(0, z) \\ + s^2 t \dot{f}(0, z) + s^2 (x - z)^2 f''(0, z)/2 + s^3 r(s, t, x, z),$$

with $s^3 r(s, t, x, z)$ the remainder. Below $a = a(0, z)$ and all the other functions are to be evaluated at $(0, z)$, unless stated otherwise. We then readily have the second order Taylor expansion of $L^{s,z}$ in s at $s = 0$:

$$(2.9) \quad L_0^z := \frac{1}{2} a^2 \partial_x^2, \quad L_1^z = L_1^z(x) := a a'(x - z) \partial_x^2 + b \partial_x,$$

and, $L_2^z = L_{2,x}^z + t L_{2,t}^z$, where

$$(2.10) \quad L_{2,x}^z := (a'^2 + a a'')(x - z)^2 \partial_x^2 / 2 + b'(x - z) \partial_x + c, \quad L_{2,t}^z := a \dot{a} \partial_x^2.$$

Hence

$$L^{s,z}(t, x) = L_0^z + s L_1^z(x) + s^2 (L_{2,x}^z(x) + t L_{2,t}^z) + s^3 L_3^{s,z}(t, x),$$

where $L_3^{s,z}(t, x)$ is the remainder term.

Remark 2.2. Each L_k^z in (2.7) has polynomial coefficients of order k in $(x - z)$ and of order $\leq k/2$ in t . In particular, L_0^z is a constant coefficient operator, for which the Green's function is computed explicitly in (2.28). Thus, in order for the expansion to capture the time dependence of the coefficients, the coefficient must be expanded at least to second order in s . Time-dependent corrections will therefore appear only at order $s^2 = t$ in the expansion of $\mathcal{G}_t^L(x, y)$.

Let \mathcal{G}_t^L be the Green function of the parabolic problem (2.1), that is, the solution is given by $U(t, x) = \int \mathcal{G}_t^L(x, y) h(y) dy =: (\mathcal{G}_t^L h)(t, x)$.

We begin the approximation scheme for \mathcal{G}_t^L by decomposing L into a constant-coefficient, second-order operator L_0 , for which we can explicitly compute the solution operator, and a remainder:

$$(2.11) \quad L(t) = L_0 + V(t)$$

where $V(t)$ is a time-dependent, variable coefficient, second order operator.

By Duhamel's principle we then have

$$(2.12) \quad \mathcal{G}_t^L = e^{tL_0} + \int_0^t e^{(t-\tau_1)L_0} V(\tau_1) \mathcal{G}_{\tau_1}^L d\tau_1.$$

Repeated applications of Duhamel's formula leads to a recursive representation of \mathcal{G}_t^L as a time-ordered expansion:

$$(2.13) \quad \begin{aligned} \mathcal{G}_t^L &= e^{tL_0} + \int_0^t e^{(t-\tau_1)L_0} V(\tau_1) e^{\tau_1 L_0} d\tau_1 \\ &\quad + \int_0^t \int_0^{\tau_1} e^{(t-\tau_1)L_0} V(\tau_1) e^{(\tau_1-\tau_2)L_0} V(\tau_2) e^{\tau_2 L_0} d\bar{\tau} + \dots \\ &\quad + \int_0^t \int_0^{\tau_1} \dots \int_0^{\tau_{d-1}} e^{(t-\tau_1)L_0} V(\tau_1) e^{(\tau_1-\tau_2)L_0} V(\tau_2) \dots V(\tau_d) e^{\tau_d L_0} d\bar{\tau} \\ &\quad + \int_0^t \int_0^{\tau_1} \dots \int_0^{\tau_{d+1}} e^{(t-\tau_1)L_0} V(\tau_1) e^{(\tau_1-\tau_2)L_0} V(\tau_2) \dots V(\tau_{d+1}) \mathcal{G}_{\tau_{d+1}}^L d\bar{\tau} \end{aligned}$$

where, for notational convenience, we have set $d\tau_k \dots d\tau_2 d\tau_1 = d\bar{\tau}$. This expansion can be rigorously justified, at least in the case when L uniformly strongly elliptic and all the coefficients of L and their derivatives are bounded. See [6, 8] for details. In the limit $d \rightarrow \infty$, it yields an asymptotic time-ordered series, also called a *Dyson series*, for the Green's function. The integer d stands for the *iteration level* in the time-ordered expansion, which at this point is distinct from the order n of the Taylor expansion of the operator L . For consistency we need $n \geq d$ [8]. We set from now on $d = n = 2$.

A similar formula holds for the Green's function $\mathcal{G}_t^{L^{s,z}}$ of the solution operator for the rescaled problem (2.5). We recall that it is enough to compute an approximate Green's function at $t = 1$ for the rescaled problem by (2.6). We now choose the operator L_0 to be exactly the zeroth-order Taylor expansion of $L^{s,z}$, given in (2.7). Then:

$$V^{s,z}(t) := L^{s,z}(t) - L_0 = sL_1^z(x) + s^2L_2^z(t, x) + s^3L_3^{s,z}(t, x).$$

and using (2.13) with $d = n = 2$ and $t = 1$ yields

$$(2.14) \quad \mathcal{G}_1^{L^{s,z}} = e^{L_0^z} + s\mathcal{I}_1^z + s^2(\mathcal{I}_{1,1}^z + \mathcal{I}_{2,x}^z + \mathcal{I}_{2,t}^z) + \mathcal{R}^{s,z},$$

where

$$(2.15) \quad \begin{aligned} \mathcal{I}_1^z &= \int_0^1 e^{(1-\tau_1)L_0^z} L_1^z e^{\tau_1 L_0^z} d\tau_1, \\ \mathcal{I}_{1,1}^z &= \int_0^1 \int_0^{\tau_1} e^{(1-\tau_1)L_0^z} L_1^z e^{(\tau_1-\tau_2)L_0^z} L_1^z e^{\tau_2 L_0^z} d\tau_2 d\tau_1, \\ \mathcal{I}_{2,x}^z &= \int_0^1 e^{(1-\tau_1)L_0^z} L_{2,x}^z e^{\tau_1 L_0^z} d\tau_1, \\ \mathcal{I}_{2,t}^z &= \int_0^1 e^{(1-\tau_1)L_0^z} \tau_1 L_{2,\tau}^z e^{\tau_1 L_0^z} d\tau_1. \end{aligned}$$

Even though we set $t = 1$, we still keep the t dependence explicit in $\mathcal{I}_{2,t}^z$ to emphasize this term comes from Taylor expansion in t . The term $\mathcal{R}^{s,z}$ in (2.14) contains all the higher order terms and will be included in the remainder.

The approximation for the Green's function \mathcal{G}_t^L of the original problem (1.1) is now obtained as follows. Let

$$(2.16) \quad T^{s,z}(x, y) =: G_0(x, y; z) + s G_1(x, y; z) + s^2 G_2(x, y; z)$$

be the distribution kernel of the operator $e^{L\tilde{z}} + s\mathcal{I}_1^z + s^2(\mathcal{I}_{1,1}^z + \mathcal{I}_{2,x}^z + \mathcal{I}_{2,t}^z)$. The desired second order approximation is then given by

$$(2.17) \quad \mathcal{G}_t^{[2]}(x, y) = t^{-1/2} T^{\sqrt{t}, z}(z + (x - z)/\sqrt{t}, z + (y - z)/\sqrt{t}),$$

where $z = z(x, y)$ is an admissible function. In particular, the kernels $G_t^{[n]}$ appearing in (1.8) are given by

$$G_t^{[n]}(x, y) := t^{-1/2} G_n(z + (x - z)/\sqrt{t}, z + (y - z)/\sqrt{t}; z(x, y)).$$

We thus need to compute the distribution kernels of the operators $e^{L\tilde{z}}$, \mathcal{I}_1^z , $\mathcal{I}_{1,1}^z$, $\mathcal{I}_{2,x}^z$, $\mathcal{I}_{2,t}^z$. In order to do so, we exploit the semigroup property of e^{tL_0} to carry out explicitly the time integration in (2.15). Before we proceed, we introduce some useful notation.

By $[T_1, T_2] := T_1 T_2 - T_2 T_1 = -[T_2, T_1]$ we shall denote the commutator of two operators T_1 and T_2 . Two operators T_1, T_2 commute if $[T_1, T_2] = 0$. For any two operators T_1 and T_2 , we define $ad_{T_1}(T_2)$ by $ad_{T_1}(T_2) := [T_1, T_2]$, and, for any integer j , we define $ad_{T_1}^j(T_2)$ recursively by

$$ad_{T_1}^j(T_2) := ad_{T_1}(ad_{T_1}^{j-1}(T_2)).$$

We next recall a Baker-Campbell-Hausdorff-type identity proved and used in this setting in [8] (note that the operators T_i are unbounded). Namely, for any $\theta \in (0, 1)$ and differential operator $Q = Q(x, \partial)$ with *polynomial coefficients* in x , we have

$$(2.18) \quad e^{\theta L_0} Q = P_{ad}(Q, \theta, x, z, \partial) e^{\theta L_0},$$

where $P_{ad}(Q, \theta, x, z, \partial)$ is a differential operator with polynomial coefficients in x given by

$$(2.19) \quad P_{ad}(Q, \theta, x, z, \partial) = Q + \sum_{i=1}^{\infty} \frac{\theta^i}{i!} ad_{L_0}^i(Q).$$

In proving this formula, we use the fact that the series is actually a finite sum, as we show below. In particular, P can be *explicitly* computed.

A simple calculation gives the following lemma.

Lemma 2.3. *Let L_m be a second-order differential operator with polynomial coefficients of degree at most m . Then $ad_{L_0}^j(L_m) = 0$ for $j > m$. In particular, we have $[L_0^z, L_{2,t}^z] = 0$, $ad_{L_0^z}^2(L_1^z) = 0$, and $ad_{L_0^z}^3(L_{2,x}^z) = 0$.*

Proof. The proof is a simple calculation. □

We now proceed to compute the integrals in (2.15)

$$\begin{aligned}\mathcal{I}_1 &= \int_0^1 e^{(1-\tau_1)L_0^z} L_1^z e^{\tau_1 L_0^z} d\tau_1 = \int_0^1 (L_1^z + (1-\tau_1)[L_0^z, L_1^z]) e^{L_0^z} d\tau_1 \\ &= (L_1^z + \frac{1}{2}[L_0^z, L_1^z]) e^{L_0^z},\end{aligned}$$

$$\begin{aligned}\mathcal{I}_{1,1} &= \int_0^1 \int_0^{\tau_1} e^{(1-\tau_1)L_0^z} L_1^z e^{(\tau_1-\tau_2)L_0^z} L_1^z e^{\tau_2 L_0^z} d\tau_2 d\tau_1, \\ &= \int_0^1 \int_0^{\tau_1} (L_1^z + (1-\tau_1)[L_0^z, L_1^z])(L_1^z + (1-\tau_2)[L_0^z, L_1^z]) e^{L_0^z} d\tau_2 d\tau_1, \\ &= (\frac{1}{2}(L_1^z)^2 + \frac{1}{3}L_1^z[L_0^z, L_1^z] + \frac{1}{6}[L_0^z, L_1^z]L_1^z + \frac{1}{8}[L_0^z, L_1^z]^2) e^{L_0^z},\end{aligned}$$

$$\begin{aligned}\mathcal{I}_{2,x} &= \int_0^1 e^{(1-\tau_1)L_0^z} L_{2,x}^z(\tau_1) e^{\tau_1 L_0^z} d\tau_1 \\ &= \int_0^1 (L_{2,x}^z + (1-\tau_1)[L_0^z, L_{2,x}^z] + \frac{(1-\tau_1)^2}{2}[L_0^z, [L_0^z, L_{2,x}^z]]) e^{L_0^z} d\tau_1 \\ &= (L_{2,x}^z + \frac{1}{2}[L_0^z, L_{2,x}^z] + \frac{1}{6}[L_0^z, [L_0^z, L_{2,x}^z]]) e^{L_0^z},\end{aligned}$$

$$\mathcal{I}_{2,t} = \int_0^1 e^{(1-\tau_1)L_0^z} \tau_1 L_{2,\tau}^z e^{\tau_1 L_0^z} d\tau_1 = \int_0^1 \tau_1 L_{2,\tau}^z e^{L_0^z} d\tau_1 = \frac{1}{2} L_{2,t}^z e^{L_0^z}.$$

Hence (2.14) becomes

$$(2.20) \quad e^{L^{s,z}} = (1 + sQ_1 + s^2Q_2) e^{L_0^z} + \mathcal{R}^{s,z},$$

where

$$(2.21) \quad \begin{aligned}Q_1 &= L_1^z + \frac{1}{2}[L_0^z, L_1^z], \\ Q_2 &= \frac{1}{2}(L_1^z)^2 + \frac{1}{3}L_1^z[L_0^z, L_1^z] + \frac{1}{6}[L_0^z, L_1^z]L_1^z + \frac{1}{8}[L_0^z, L_1^z]^2, \\ &\quad + L_{2,x}^z + \frac{1}{2}[L_0^z, L_{2,x}^z] + \frac{1}{6}[L_0^z, [L_0^z, L_{2,x}^z]] + \frac{1}{2}L_{2,t}^z,\end{aligned}$$

and $\mathcal{R}^{s,z}$ is again the error term as in (2.14). Therefore, we only need to compute the commutators in the above formula to get the second-order approximation of $\mathcal{G}_t^{L^{s,z}}$.

We recall that we agreed that all functions in the commutator formulas below are evaluated at $(0, z)$. Hence $a = a(0, z)$, $a' = a'(0, z)$, and so on. We have

$$(2.22) \quad [L_0^z, L_1^z] = a(0, z)^3 a'(0, z) \partial_x^3 = a^3 a' \partial_x^3, \quad [L_0^z, L_1^z]^2 = a^6 a'^2 \partial_x^6,$$

and hence

$$(2.23) \quad \begin{aligned} L_1^z[L_0^z, L_1^z] &= a^4 a'^2 (x-z) \partial_x^5 + b a^3 a' \partial_x^4, \\ [L_0^z, L_1^z] L_1^z &= a^4 a'^2 (x-z) \partial_x^5 + (b + 3a a') a^3 a' \partial_x^4. \end{aligned}$$

To compute the other commutators, we need the following lemma, which can be proved by induction using that $[AB, C] = A[B, C] + [A, C]B$. In particular, $[\partial_x^2, x-z] = 2\partial_x$ and $[\partial_x^2, (x-z)^2] = 2 + 4(x-z)\partial_x$.

Lemma 2.4. *For $i, j \geq 1$ integers we have*

$$\partial_x^i (x-z)^j u(x) = \sum_{k=0}^{\min\{i,j\}} k! \binom{i}{k} \binom{j}{k} (x-z)^{j-k} \partial_x^{j-k} u(x).$$

We therefore have:

$$(2.24) \quad \begin{aligned} [L_0^z, L_{2,x}^z] &= a^2 (a'^2 + a a'') (x-z) \partial_x^3, \\ &+ a^2 (b' + a'^2/2 + a a''/2) \partial_x^2, \end{aligned}$$

and hence

$$(2.25) \quad [L_0^z, [L_0^z, L_{2,x}^z]] = a^4 (a'^2 + a a''), \partial_x^4,$$

so that finally

$$(2.26) \quad (L_1^z)^2 = (a a' (x-z))^2 \partial_x^4 + 2(a^2 a'^2 + a a' b) (x-z) \partial_x^3 + (a a' b + b^2) \partial_x^2.$$

It follows that the approximation kernel of $\mathcal{G}_1^{L^s, z}$ is given by the applications of a differential operator with polynomial coefficients to the Green's function of e^{tL_0} . If ϕ is a smooth function, we denote by C_ϕ the convolution operator with ϕ , then $C_\phi f(x) := \phi * f(x) = \int \phi(x-y) f(y) dy$, which shows that the distribution kernel of C_ϕ is $C_\phi(x, y) = \phi(x-y)$. It is immediate to check that

$$(2.27) \quad \partial_x C_\phi = C_{\partial_x \phi},$$

while $C_\phi \partial_x = -C_{\partial_x \phi}$. By Remark 2.2, the distribution kernel of $e^{L_0^z}$ is given by

$$(2.28) \quad e^{L_0^z}(x, y) = \frac{1}{\sqrt{2\pi a^2}} \exp\left(-\frac{|x-y|^2}{2a^2}\right), \quad a = a(0, z),$$

and hence $e^{L_0^z}$ is a convolution operator.

Then, by (2.27) $\partial_x^k e^{L_0^z}(x, y) = H_k(\Theta) e^{L_0^z}(x, y)$, where $\Theta = \frac{x-y}{a^2}$ and H_k are the (rescaled Hermite) polynomials satisfying $H_0 = 1$ and $H_{k+1}(\Theta) = -\Theta H_k(\Theta) + H'_k(\Theta)/a^2$. The polynomials H_k are easily computed by induction as:

$$(2.29) \quad \begin{aligned} H_1(\Theta) &= -\Theta, \quad H_2(\Theta) = \Theta^2 - \frac{1}{a^2}, \quad H_3(\Theta) = -\Theta^3 + \frac{3\Theta}{a^2}, \\ H_4(\Theta) &= \Theta^4 - \frac{6\Theta^2}{a^2} + \frac{3}{a^4}, \quad H_5(\Theta) = -\Theta^5 + \frac{10}{a^2} \Theta^3 - \frac{15\Theta}{a^4}, \\ H_6(\Theta) &= \Theta^6 - \frac{15}{a^2} \Theta^4 + \frac{45}{a^4} \Theta^2 - \frac{15}{a^6}. \end{aligned}$$

Using (2.29) we have

$$(2.30) \quad G_0(x, y; z) = e^{L\tilde{z}} = \frac{1}{\sqrt{2\pi a^2}} \exp\left(-\frac{|x-y|^2}{2a^2}\right),$$

and

$$(2.31) \quad \begin{aligned} G_1(x, y; z) &= \left((L_1 + \frac{1}{2}[L_0, L_1])e^{L_0} \right)(x, y) \\ &= \left(b\partial_x + aa'(x-z)\partial_x^2 + \frac{1}{2}a^3a'\partial_x^3 \right) e^{L\tilde{z}}(x, y) \\ &= \left(bH_1(\Theta) + aa'(x-z)H_2(\Theta) + \frac{1}{2}a^3a'H_3(\Theta) \right) e^{L\tilde{z}} \\ &= \frac{1}{\sqrt{2\pi a^2}} e^{-\frac{|x-y|^2}{2a^2}} \left[\left(\frac{3aa' - 2b}{2a^2} \right) (x-y) - \frac{a'}{2a^3}(x-y)^3 \right. \\ &\quad \left. + (x-z) \left(\frac{(x-y)^2 - a^2}{a^3} \right) \right]. \end{aligned}$$

We now carry out a similar calculation for the next (and last) term of our asymptotic expansion, namely

$$(2.32) \quad G_2(x, y; z) = (Q_2 e^{L\tilde{z}})(x, y),$$

with Q_2 given by Equation (2.21). We finally have

$$(2.33) \quad \begin{aligned} G_2(x, y; z) &= \left(\frac{1}{2}L_{2,\tau}^z + L_{2,x}^z + \frac{1}{2}[L_0^z, L_{2,x}^z] + \frac{1}{6}[L_0^z, [L_0^z, L_{2,x}^z]] \right. \\ &\quad \left. + \frac{1}{2}L_1^{z,2} + \frac{1}{3}L_1^z[L_0^z, L_1^z] + \frac{1}{6}[L_0^z, L_1^z]L_1^z + \frac{1}{8}[L_0^z, L_1^z]^2 \right) e^{L\tilde{z}} \\ &= \left(P_0 + \sum_{i=1}^6 P_i H_i(\Theta) \right) e^{L\tilde{z}}(x, y). \end{aligned}$$

where P_j are polynomials in $x-z$ and $x-y$ with coefficients given in terms of the values of the functions a , b , and c , and their derivatives, all evaluated at $z = z(x, y)$, as follows

$$(2.34) \quad \begin{aligned} P_0 &= c, \quad P_1 = b'(x-z), \\ P_2 &= \frac{1}{2} \left[\frac{1}{2}a^3a'' + a^2b' + a^2a'^2/2 + b^2 + a'^2(x-z)^2 \right. \\ &\quad \left. + a(ba' + \dot{a} + a''(x-z)^2) \right], \\ P_3 &= a(x-z)(a'b + \frac{1}{2}a^2a'' + \frac{3}{2}aa'^2), \\ P_4 &= \frac{a^2}{3} \left[\frac{1}{2}a^3a'' + 2a^2a'^2 + a\frac{3}{2}a'b + \frac{3}{2}a'^2(x-z)^2 \right], \\ P_5 &= \frac{1}{2}a^4a'^2(x-z), \quad P_6 = \frac{1}{8}a^6a'^2. \end{aligned}$$

In particular, we obtain the following explicit formula.

Example 2.5. For the CEV model given by Equation (1.3), we have $a = \sigma z^\alpha$, $a' = \alpha \sigma z^{\alpha-1}$, $b = rz^\alpha$, $z = z(x, y)$, and hence,

$$G_1^{CEV}(x, y; z) = \frac{1}{\sigma z^\alpha \sqrt{2\pi}} \left[\left(\frac{3\alpha\sigma^2 z^{2(\alpha-1)} - 2r}{2\sigma} \right) \left(\frac{x-y}{\sigma z^\alpha} \right) - \frac{\alpha\sigma z^{\alpha-1}}{2} \left(\frac{x-y}{\sigma z^\alpha} \right)^3 + \left(\frac{x-z}{\sigma z^\alpha} \right) \left(\left(\frac{x-y}{\sigma z^\alpha} \right)^2 - 1 \right) \right] e^{-\frac{|x-y|^2}{2\sigma^2 z^{2\alpha}}}.$$

Let us introduce the *time dependent Black-Scholes-Merton model* to correspond to the operator

$$(2.35) \quad L := \frac{1}{2}\sigma(t)^2 x^2 \partial_x^2 + r(t)x\partial_x - r(t),$$

Thus the difference between the usual Black-Scholes-Merton model (1.2) and the time dependent Black-Scholes-Merton model (2.35) is that in the latter we allow σ and r to depend on time. Then the asymptotic formula for the time dependent Black-Scholes-Merton model is obtained by setting $\alpha = 1$ in the Example 2.5, since that formula does not contain time derivatives of the coefficients.

At this stage, we can allow the basepoint z to vary with x and y . In Section 2.1 below we compute the expansion for the basepoint $z(x, y) = x$ and compare it in Section 4. Different choices of basepoints z may lead to more accurate and stable approximations. In future work, we plan to study how to optimize the choice of z .

Definition 2.6. We call a function $z = z(x, y)$ admissible if $z(x, x) = x$ and all derivatives of z are bounded.

In [6, 8], we rigorously prove error bounds for the remainder term in (1.13) in Sobolev spaces under the assumption that z be admissible (and all the coefficients of L , together with their derivatives, be bounded functions, and L be uniformly strongly elliptic). The function $z = z(x, y)$ can be thus quite general.

2.1. Kernel expansions at $z = x$. The choice $z = x$ yields a simplified expression for the approximation, since certain terms disappear, and the approximation yields the price of a European call option in closed form. In fact, the convolution with the approximate Green's function can be evaluated exactly and the price of a European call option given in closed form. In particular there is no need for numerical quadrature in evaluating the integrals, thus improving the speed of our calculations.

Example 2.7. By setting $z = x$ in (2.31) and evaluating all coefficient functions at $(0, x)$, we obtain the first-order correction to the rescaled kernel $\mathcal{G}_1^{L^{s,z}}$ in the form:

$$(2.36) \quad G_1(x, y; z = x) = \frac{x-y}{\sqrt{2\pi a^2}} e^{-\frac{(x-y)^2}{2a^2}} \left(\frac{3aa' - 2b}{2a^2} - \frac{a'}{2a^3} (x-y)^2 \right).$$

Example 2.8. Similarly, the second-order correction to the rescaled kernel $G_1^{L^{s,z}}$ is obtained in the form:

$$(2.37) \quad G_2(x, y; z = x) = \frac{1}{\sqrt{2\pi a^2}} e^{-\frac{(x-y)^2}{2a^2}} \cdot \left\{ \frac{1}{8} a^6 a'^2 H_6(\Theta) + \frac{a^3}{6} (a^2 a'' + 4aa'^2 + 3ba') H_4(\Theta) + \frac{1}{4} (a^3 a'' + 2a^2 b' + 2a\dot{a} + 2aa'b + a'^2 a^2 + 2b^2) H_2(\Theta) + c \right\},$$

where $\Theta = \frac{x-y}{a(0,x)}$, and H_6, H_4, H_2 are given by (2.29).

Example 2.9. For the time-dependent Black-Scholes-Merton equation, we have $b(t, x) = r x$, $c(t, x) = -r$ and $a(t, x) = \sigma(t) x$ so that

$$(2.38) \quad G_1^{BSM}(x, y; z = x) = \frac{x-y}{\sqrt{2\pi\sigma^2 x^2}} e^{-\frac{1}{2}\left(\frac{x-y}{\sigma x}\right)^2} \left[\frac{3\sigma^2 - 2r}{2\sigma} - \frac{\sigma}{2} \left(\frac{x-y}{\sigma x}\right)^2 \right],$$

where all coefficient functions are calculated at $(0, x)$.

Example 2.10. The second-order correction to the rescaled kernel is given by

$$(2.39) \quad G_2^{BSM}(x, y; z = x) = \frac{1}{\sqrt{2\pi\sigma x}} e^{-\frac{1}{2}X^2} \cdot \left[-\frac{\sigma^4 + 4\sigma\dot{\sigma}(0) + 4r^2 + 4r\sigma^2}{8\sigma^2} + \frac{4\dot{\sigma}(0)\sigma + 4r^2 - 16r\sigma^2 + 15\sigma^4}{8\sigma^2} X^2 + \frac{12r - 29\sigma^2}{24} X^4 + \frac{\sigma^2}{8} X^6 \right],$$

where $X = (x-y)/(\sigma x)$.

Example 2.11. For the time-dependent CEV model, $c(t, x) = -r$ and $a(t, x) = \sigma(t) x^\alpha$, $b(t, x) = r x$ with $\sigma(0) = \sigma$ so that

$$(2.40) \quad G_1^{CEV}(x, y; z = x) = \frac{x-y}{\sqrt{2\pi\sigma^2 x^{2\alpha}}} e^{-\frac{1}{2}\left(\frac{x-y}{\sigma x^\alpha}\right)^2} \left[\frac{3\alpha\sigma^2 x^{\alpha-1} - 2rx^{1-\alpha}}{2\sigma} - \frac{\alpha\sigma x^{\alpha-1}}{2} \left(\frac{x-y}{\sigma x^\alpha}\right)^2 \right],$$

and

Example 2.12. For the second order correction we have

$$(2.41) \quad G_2^{CEV}(x, y; z = x) = (P_2 H_2 + P_4 H_4 + P_6 H_6 - r) \frac{1}{\sqrt{2\pi\sigma x^\alpha}} \cdot e^{-\frac{(x-y)^2}{2\sigma^2 x^{2\alpha}}}$$

where

$$H_2 = \left(\frac{x-y}{\sigma^2 x^{2\alpha}}\right)^2 - \frac{1}{\sigma^2 x^{2\alpha}}, \quad H_4 = \left(\frac{x-y}{\sigma^2 x^{2\alpha}}\right)^4 - \frac{6(x-y)^2}{\sigma^6 x^{6\alpha}} + \frac{3}{\sigma^4 x^{4\alpha}}$$

$$H_6 = \left(\frac{x-y}{\sigma^2 x^{2\alpha}}\right)^6 - \frac{15}{\sigma^2 x^{2\alpha}} \left(\frac{x-y}{\sigma^2 x^{2\alpha}}\right)^4 + \frac{45}{\sigma^4 x^{4\alpha}} \left(\frac{x-y}{\sigma^2 x^{2\alpha}}\right)^2 - \frac{15}{\sigma^6 x^{6\alpha}}$$

and

$$P_2 = \frac{1}{4} (\sigma^4 \alpha (2\alpha - 1) x^{4\alpha-2} + 2\sigma(\sigma r + \dot{\sigma}(0) + \sigma \alpha r) x^{2\alpha} + 2r^2 x^2)$$

$$P_4 = \frac{1}{6} \sigma^4 \alpha x^{4\alpha} (\sigma^2 (\alpha - 1) x^{2\alpha-2} + 4\sigma^2 \alpha x^{2\alpha-2} + 3r), P_6 = \frac{1}{8} \sigma^8 \alpha^2 x^{8\alpha-2}$$

Note that in the above two Examples for the CEV model, setting $\alpha = 1$ leads to the corresponding approximation for the BSM model.

3. CLOSED FORM APPROXIMATE SOLUTIONS

In this section, we consider European call options. For European put options similar results can also be obtained, either directly from the definition or by using put-call parity [32]. In what follows, we will work with the expansion obtained by setting $z(x, y) = x$ as the basepoint. In this case, we are able to compute the integrals defining the approximate option price $U^{[k]}$ from $G^{[k]}$ in closed form, which bypasses the need for more computationally intensive integration methods such as numerical quadrature, which are needed for more general basepoints z .

By (2.36) and (2.6), the first-order approximate Green's function is given by

$$(3.1) \quad \mathcal{G}_t^{[1]}(x, y) = \frac{1}{\sqrt{2\pi t a}} e^{-\frac{(x-y)^2}{2a^2 t}} \left(1 + \frac{3aa' - 2b}{2a^2} (x-y) - \frac{a'}{2a^3 t} (x-y)^3 \right).$$

Similarly, by (2.37) and (2.6) the second-order approximate Green's function is given by

We recall that we implicitly assume all coefficients are evaluated at $(0, x)$.

$$(3.2) \quad \mathcal{G}_t^{[2]}(x, y) = \frac{\sqrt{t}}{\sqrt{2\pi a}} e^{-\frac{(x-y)^2}{2a^2 t}} \cdot (P_6 H_6(\Xi) + P_4 H_4(\Xi) + P_2 H_2(\Xi) - r)$$

where $\Xi = \frac{x-y}{a^2 \sqrt{t}}$, the functions H_6, H_4, H_2 are given by (2.29), and

$$(3.3) \quad \begin{aligned} P_6 &= \frac{1}{8} a^6 a'^2, P_4 = \frac{a^3}{6} (a^2 a'' + 4aa'^2 + 3ba') \\ P_2 &= \frac{1}{4} (a^3 a'' + 2a^2 b' + 2aa' + 2aa'b + a'^2 a^2 + 2b^2) \end{aligned}$$

All the coefficient functions are evaluated at $t = 0, z = x$.

For European Call options with strike price K , by (1.5) the n^{th} - order approximated option price is

$$(3.4) \quad U^{[n]}(t, x) = \int_0^\infty \mathcal{G}_t^{[n]}(x, y) (y - K)^+ dy,$$

where we only take $n = 1, 2$ here. We recall that $t = T - \mathfrak{t}$ is the time to expiry T and \mathfrak{t} is real time. So to be more precise, *the n^{th} -order option pricing formula for European call options with expiry time T is $U^{[n]}(T - \mathfrak{t}, x)$.*

We have already observed that the general form of the approximate kernel, when $z = x$, is a product of polynomial functions against a rescaled Gaussian. Therefore, the integration in (3.4) above can be carried out in terms of error functions. Explicitly,

$$U^{[1]}(t, x) = \frac{\sqrt{t}}{2\sqrt{2\pi}} e^{-\frac{(x-K)^2}{2a^2t}} (2a - a'(x-K)) + \frac{1}{2} \cdot \left(\operatorname{erf} \left(\frac{x-K}{\sqrt{2ta}} \right) + 1 \right) (bt + x - K),$$

and

$$(3.5) \quad \begin{aligned} U^{[2]}(t, x) = & U^{[1]}(t, x) + \frac{rt}{2} \left(\operatorname{erf} \left(\frac{x-K}{a\sqrt{2t}} \right) + 1 \right) (K-x) \\ & + \frac{1}{2\sqrt{2\pi t}} e^{-\frac{(x-K)^2}{2a^2t}} \cdot \left(\frac{t^2}{6} a^2 a'' - a(r + a'^2/12) t^2 \right. \\ & + (t\dot{a} + a''(x-K)^2/3) t + \frac{t}{a} (tb^2 - a'^2(x-K)^2/6) \\ & \left. + \frac{tba'(x-K)^2}{a^2} + \frac{a'^2(x-K)^4}{4a^3} \right), \end{aligned}$$

Note that in financial applications (*i.e.*, in the risk free measure) $b(t, x) = rx$ and $c(t, x) = -r$.

Example 3.1. *For the CEV model we have*

$$(3.6) \quad \begin{aligned} U_{CEV}^{[1]}(t, x) = & \frac{\sigma x^{\alpha-1} \sqrt{t}}{2\sqrt{2\pi}} e^{-\frac{(x-K)^2}{2\sigma^2 t x^{2\alpha}}} ((2-\alpha)x + \alpha K) \\ & + \frac{1}{2} \cdot \left(\operatorname{erf} \left(\frac{x-K}{\sqrt{2t\sigma x^\alpha}} \right) + 1 \right) ((1+rt)x - K). \end{aligned}$$

and when $\alpha = 1$, it reduces to the first order approximation for the Black-Scholes-Merton model.

4. COMPARISON AND PERFORMANCE OF THE METHOD

In this section, we discuss the accuracy and efficiency of our approximation for the Black-Scholes-Merton and the CEV model. We employ the Black-Scholes-Merton model primarily as a didactic example, given that an exact kernel and option pricing formulas exists. For the CEV model, we compare our approximation to other solution formulas considered a benchmark in the literature, in particular the Hagan-Woodward scheme [19].

What we find in general is a very good agreement of the approximate pricing formulas we derive in this paper with those available in the literature, but with significant advantage in the computational efficiency. In particular, the agreement is good even for times that are not small. In Section 5,

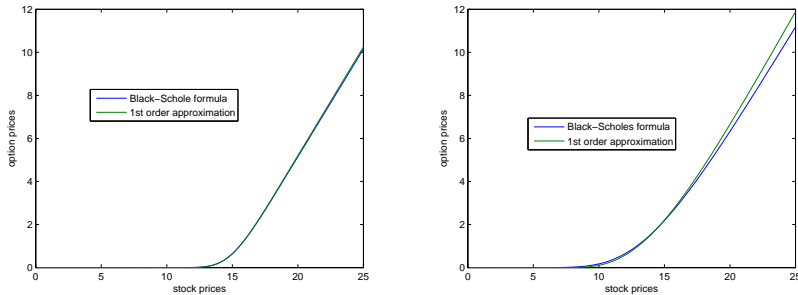


FIGURE 1. Comparison of our first order approximation with the Black-Scholes formula. Parameters: $K = 15$, $\sigma = 0.3$, $r = 0.1$. Basepoint $z = x$. The left picture is for $t = 0.1$, and the right one is for $t = 0.8$. Note that the x-axis is scaled by 10, i.e. the label 150 means the stock price is 15.

we propose a bootstrap scheme in time to improve the accuracy of our approximation for large time.

4.1. Performance of the method. We start by discussing the Black-Scholes-Merton model, and choose the parameters $K = 15$, $\sigma = 0.3$ and $r = 0.1$, and plot the exact and approximate solutions for $0 < x < 25$. We compare our formula with the Black Scholes exact solution formula for different times t . Figure 1 gives two different cases, which show that when t is small the two solutions are in very good agreement with an absolute error of order $O(10^{-3})$. We notice that even when t is not small, the error is small. Tables 1 and 2 give a analysis of the *pointwise* error for the first order approximation with respect to the exact Black-Scholes formula.

Remark 4.1. Throughout this section, we *fix the basepoint* $z = x$, so that we have closed-form approximate solution formulas, and we can better gauge the error introduced by the our method. For more general basepoints z , further error is introduced by the numerical quadrature used for the integration and the truncation of the pay-off function h at large x (this error is lower order, however, if h is truncated at x large enough with respect to K).

Remark 4.2. Formula (??) shows that the first-order approximation of the kernel depends linearly on rt . Therefore, the error grows more rapidly for r large at comparable times. The same observation holds for the CEV model. For Black-Scholes, this issue does not arise, since a change of variables allows to reduce to the case $r = 0$ in the equation.

Analytic pricing formulas for the CEV model in terms of Bessel function series have been derived for any value of β [9,13]. However, sum such series to

$t \backslash x$	12	13	14	15	16	17	18
0.01	0.0000	0.0000	0.0313	0.3266	0.0387	0.0019	0.0000
0.05	0.0461	0.3385	0.0179	0.3915	0.0179	0.4068	0.3957
0.1	0.7	0.7	0.2	0.5	0.2	0.4	1.2
0.2	2.2	0.3	0.7	0.9	0.7	0.3	1.3
0.5	1.2	2.1	2.5	2.7	2.7	2.9	1.9

TABLE 1. Error of the first order approximation for the BSM model, $K = 15, \sigma = 0.3, r = 0$, error scale= 10^{-3} .

$t \backslash x$	12	13	14	15	16	17	18
0.01	0.0000	0.0000	0.1000	0.0000	0.9000	2.0000	3.0000
0.05	0.1	0.9	1.4	0.1	3.6	8.7	14.5
0.1	1.7	3.8	3.3	0.3	7.0	15.9	26.4
0.2	9.3	10.7	7.1	1.2	14.0	30.2	48.8
0.5	39.0	31.4	15.1	8.4	39.4	76.0	116.8

TABLE 2. Error of the first order approximation for the BSM model, $K = 15, \sigma = 0.3, r = 0.1$, error scale= 10^{-3} .

accurate order can be very computationally intensive (but see Schroder [31] for methods to compute the pricing formulas more efficiently).

The numerical tests show our approach yields accurate pricing formulas that are, however, computationally much simpler. We choose $\beta = \frac{2}{3}, K = 15, \sigma = 0.3, r = 0.1$ for parameters. Schroder [31] derived the exact CEV solution when $\beta = \frac{2}{3}$. Figure 2 gives the comparison of our method and the true solution of the CEV model for this value of β for different times. Again, we plot the two solutions for $0 < x < 25$.

Hagan and Woodward in [19] studied more general local volatility models, for which the stock price under the forward measure follows the SDE

$$dF_t = \gamma(t)A(F_t)dW_t,$$

for some deterministic and suitably smooth functions γ and A . CEV fits into this general model.

Using a singular perturbation technique, Hagan and Woodward obtain a very accurate formula for the implied volatility for this model. In the CEV case, their implied volatility reads

$$\sigma_B = \frac{a}{f^{1-\beta}} \left(1 + \frac{1}{24}(1-\beta)(2+\beta) \left(\frac{e^{rT}S_0 - K}{f} \right)^2 + \frac{1}{24} \frac{(1-\beta)^2 a^2 T}{f^{2(1-\beta)}} \right),$$

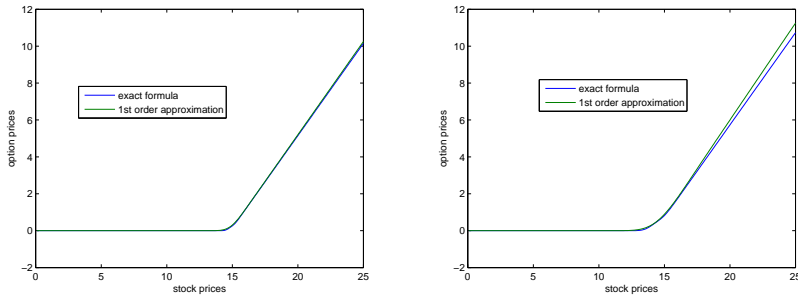


FIGURE 2. Comparison of our first order approximation with the exact formula for the CEV model derived in [31]. Parameters: $\beta = \frac{2}{3}$, $K = 15$, $\sigma = 0.3$, $r = 0.1$. Basepoint $z = x$. The first graph is plotted when $t = 0.1$, and the second is when $t = 0.5$. In the graphs the x-axis is scaled by 10, i.e the label 150 means the stock price is 15.

where

$$a = \sigma \sqrt{\frac{e^{2r(1-\beta)T} - 1}{2r(1-\beta)T}}, f = \frac{e^{rT} S_0 + K}{2}.$$

The approximate pricing formula is then obtained from the Black-Scholes formula by using σ_B as volatility.

When $\beta = \frac{2}{3}$, the CEV formula can be computed exactly [31]. In this case, Hagan and Woodward's approximation is shown by Corielli *et al* to be very accurate [7]. We therefore take this approximation as benchmark for comparison with our method. In the following numerical comparison, we choose $\beta = 2/3$, $K = 20$, $r = 0.1$, $\sigma = 0.3$ and different times $\tau = 0.3, 0.5$. We compute the prices on the interval $[0, 30]$, and divide it into 300 subintervals. Since the prices near the strike is of most interest for practitioners, we compare the methods near $K = 20$. Figure 3 gives the results, from which we see that our approximation is more accurate than the Hagan-Woodward approximation near the strike for different times.

We remark that our method can in principle yield arbitrary accuracy in the small-time limit if more terms in the kernel expansion (1.8) are included. Furthermore, it allows to derive approximate solution formulas for even more general models than those of Hagan and Woodward.

4.2. The Greeks. In this part, we use the second-order approximate solution to compute the Greeks of a European call option. The Delta and Gamma of a call option, collectively known as the *Greeks* of the option, at the point x are calculated as

$$\text{delta} = \frac{u(\tau, x + dx) - u(\tau, x - dx)}{2dx},$$

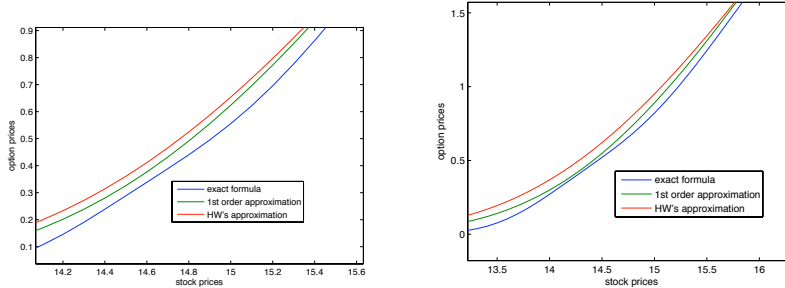


FIGURE 3. Comparison of our approximation with Hagan's results for the CEV model near strike. Parameters: $\beta = 2/3$, $K = 20$, $r = 0.1$, $\sigma = 0.3$. Basepoint: $z = x$. The first graph is plotted when $t = 0.3$, and the second is when $t = 0.5$. Note that in the graphs the x-axis is scaled by 10, i.e. the label 200 denotes that the stock price is 20.

and

$$\text{gamma} = \frac{u(\tau, x + dx) + u(\tau, x - dx) - 2u(\tau, x)}{dx^2}$$

respectively, where $u(t, x)$ is the option price. Some methods, for example the Monte Carlo method, can price options accurately, but they are not efficient for obtaining good hedging parameters. We shall show that our approximations not only give option prices, but also Greeks accurately. Again for didactic purposes, we choose the Black-Scholes-Merton model for which the Greeks can be computed exactly.

Since we can price options in closed form (by choosing $z = x$), we can calculate the Greeks in closed form by simply differentiating the approximate pricing formula. However, again because of the complexity of these formulas, we will obtain the hedging parameters numerically.

In the numerical experiment, we choose the parameters as follows: maturity $\tau = 0.5$, volatility $\sigma = 0.5$, strike $K = 20$, interest rate $r = 10\%$. In Figure 4, we plot the difference between our approximation and the exact solution for Delta when the stock price varies from 0 to 40. Figure 5 does the same for Gamma. The numerical test shows that the pointwise difference is very small, of the order of 10^{-3} in both cases. More specifically, the biggest error is around 13×10^{-3} .

5. OPTION PRICING WITH LONG MATURITY: THE BOOTSTRAP SCHEME

The Dyson-Taylor commutator method gives an asymptotic expansion of the Green function *in the limit* $t \rightarrow 0$. Therefore, its accuracy is in principle limited to times to maturity t relatively small. For long maturity options, we expect the error to be possibly large. In this section, we shall introduce a bootstrap strategy to price options with a long maturity time. The scheme

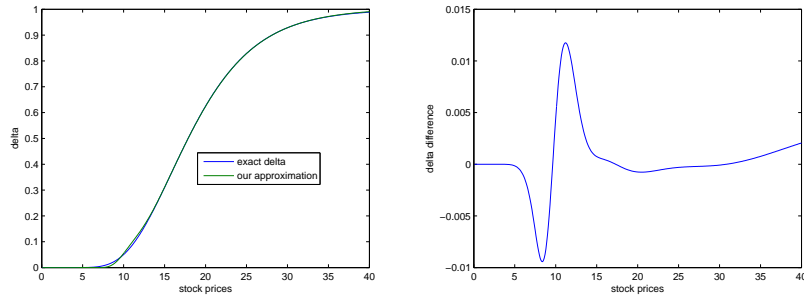


FIGURE 4. Comparison of Delta of our approach and the true values under the Black-Scholes model. Model parameters: $t = 0.5, K = 20, \sigma = 0.5, r = 10\%$. Basepoint: $z = x$. The left graph plots the delta computed by our method and the true delta. The right graph plots their difference. Note that in the second figure the scale is 10^{-3} . The x-axis is scaled by 10, that is, the label 400 means the stock price is 40.

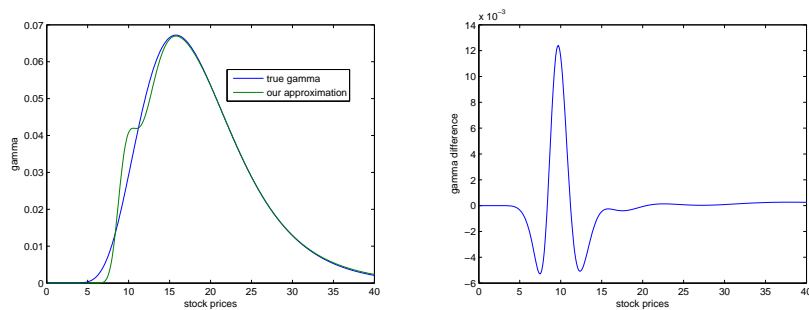


FIGURE 5. Comparison of Gamma of our approach and the true values under the Black-Scholes model. Model parameters: $t = 0.5, K = 20, \sigma = 0.5, r = 10\%$. Basepoint: $z = x$. The left graph plots the gamma computed by our method and the true gamma. The right graph plots their difference. Note that in the second figure the scale is 10^{-3} . The x-axis is scaled by 10, that is, the label 400 means the stock price is 40.

is based on the properties of the solution operator. Let us illustrate the bootstrap in the time independent case. In this case, we recall that the solution operator forms a semigroup. The semigroup property then gives that

$$(5.1) \quad e^{tL} = \left(e^{\frac{t}{n}L} \right)^n, \quad \forall n \in \mathbb{N}.$$

Then, if n is sufficiently large, $e^{\frac{t}{n}L}$ will be accurately approximated by our method.

We next describe the bootstrap scheme, which can be rigorously justified at least for the case of strongly elliptic operators (a bounded away from zero) by the error analysis in [8]. In the bootstrap scheme, we use $\left(\mathcal{G}_{t/n}^{[n]}\right)^n$ to approximate e^{tL} , where as before we denote the approximate solution operator by its kernel $\mathcal{G}_t^{[n]}$. Suppose now $\mathcal{G}_{t/n}^{[n]}$ is the second order approximation, then the error is in the order $O\left(\left(\frac{t}{n}\right)^{3/2}\right)$. Because there are n steps in the bootstrap scheme, the total error is in the order of

$$O\left(\left(\frac{t}{n}\right)^{3/2}\right) \times n = O\left(t^{3/2}/\sqrt{n}\right),$$

and consequently, for t fixed, it becomes smaller and smaller as n increases. A similar analysis shows that the bootstrap strategy with the first order approximation does not improve accuracy, given that in this case the error at each step is $O(t/n)$, so the total error after n steps is

$$O(t/n) \times n = O(t),$$

which does not converge to zero as $n \rightarrow \infty$.

We numerically tested this scheme for both the option prices and the Greeks. In the bootstrap scheme, closed-form approximate solutions are not available after the first time step, since we integrate the approximate Green's function against an expression of the form (3.5), which contains error functions. Therefore, we must integrate numerically and introduce an additional error due to the numerical quadrature. This error can be controlled and made lower-order by choosing the space discretization step small enough. A further error, which can also be made lower-order, comes from the truncation of the integration at large x .

In the first simulation, we used the Black-Scholes-Merton model. and set the parameters as time to maturity $t = 1$ (one year), strike $K = 20$, risk-free interest rate $r = 10\%$, and volatility $\sigma = 0.5$. The left graph of Figure (6) displays the error of the first-order-closed form solution, the second-order closed-form solution, the first-order approximation with bootstrap, and the second-order approximation with bootstrap. We truncate the half line $(0, +\infty)$ at 200, and fix the number of the bootstrap steps as $n = 10$, that is the time step is $\Delta t = 0.1$. We choose the space discretization $\Delta x = 0.1$. From the graphs, it is clear that the second-order approximation greatly improves the accuracy compared with the first-order approximation. The bootstrap scheme with the second-order approximation reduces the error even further as expected (See Table 3 for a quantitative error analysis). As predicted, on the other hand the bootstrap scheme with the first order approximation introduces an extra error.

We also notice that around $S = 40$ (the label 400 in the graphs) the error with the second-order bootstrap tends to increase, an effect of the truncation error. To verify it, we truncate the half line at 400. The right

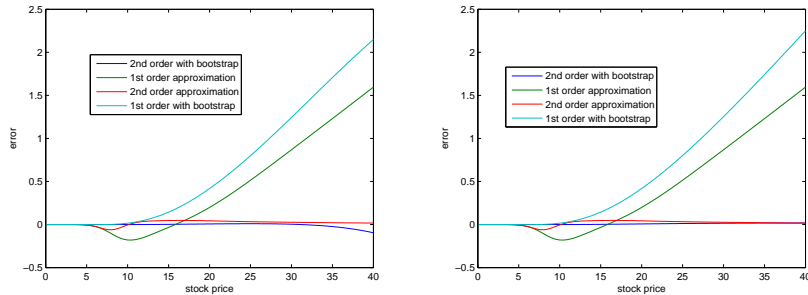


FIGURE 6. Comparison of our first and second order approximation with or without bootstrap. Each curve is the difference with respect to the Black-Scholes formula. Parameters: $t = 1, K = 20, r = 10\%, \sigma = 0.5$. Basepoint: $z = x$. In our numerical integration, we truncate $(0, \infty)$ at 200 for the left picture, and at 400 for the right one. Note that the x-axis scaled by 10, i.e. the label 400 means the stock price is 40.

t	3	2	1	0.5	0.2	0.1
error	0.0268	0.0379	0.0177	0.0038	4.3682e-004	3.5703e-005

TABLE 3. Errors of the bootstrap scheme for different times under the Black-Scholes-Merton model. Number of bootstrap steps is fixed as 10. Parameters: $K = 20, \sigma = 0.5, r = 10\%$. Errors are measured in $L^\infty(0, 40)$, and the benchmark is the Black-Scholes formula

graph of Figure (5) shows that the error does not tend to increase. We also tested the cases when the time to maturity is two and five years, obtaining similar results.

To give a sense on how accurate our bootstrap scheme with the second order approximation is for large time to maturity, we repeat previous numerical simulation for difference times, and measure the error in $L^\infty(0, 40)$. We recall that the trike price is at $S = 20$, we are taking a symmetric interval around it, and that the number of bootstrap steps is fixed at 10. We report the errors in Table 3.

As predicted, we can increase the number of bootstrap steps to obtain arbitrary accuracy in the approximation. Furthermore, for relatively large t the number of bootstrap steps should be correspondingly large, so that the compound error from each bootstrap step is under control at the end. For example, in our tests when $t \geq 4$, it is not enough to reduce the error by bootstrapping with 10 steps. Using only 10 steps in this case, in fact, introduces additional errors. For more detail, see [6].

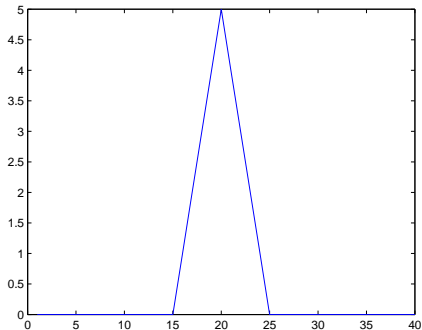


FIGURE 7. Butterfly option payoff.

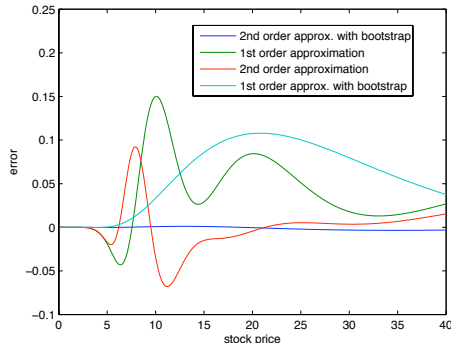


FIGURE 8. comparison of our first order and second order approximation with or without bootstrap for a butterfly option when $t = 1, r = 10\%, \sigma = 0.5$. In our numerical integration we truncate the half line at 200. Note that the x-axis is scaled by 10, i.e. the label 40 means the stock price is 40.

In order to eliminate the effect of the truncation error, we shall work with a butterfly option in the rest of this section. Mathematically, a butterfly option corresponds to an initial pay-off given by a hat function, Figure (7). Our method gives closed-form solution for butterfly options as well, by linearity. Figure (8) shows the errors of a butterfly option within the Black-Scholes-Merton model with $K = 20, K_1 = 15, K_2 = 25$ obtained by our first order and second order approximation with or without bootstrap. The benchmark is the true solution. The parameters we were using are the same as we mentioned before. Again, we truncate the half line at 200. For a butterfly option, the truncation error is clearly very small, given that the data is compactly supported (Figure (8)). For the second order approximation with a bootstrap scheme, the error is almost zero. It is in the scale of 10^{-3} , while without the bootstrap the error is of the scale 10^{-2} . This coincides with our theoretical results.

We can also run the simulation as in Table 3, and we find comparable results.

We conclude by discussing the bootstrap scheme for the Greeks. Directly using the closed-form approximation formula to compute the Greeks for very long maturity time ($t \gg 1$) is not advisable. In fact, our closed-form approximation for call option oscillates near the strike price, and the oscillation grows with the time to expiry, as the overall error grows. The appearance of the oscillation is due to the discontinuity of first derivative of the pay-off function at the strike price. This phenomenon is clearly visible for

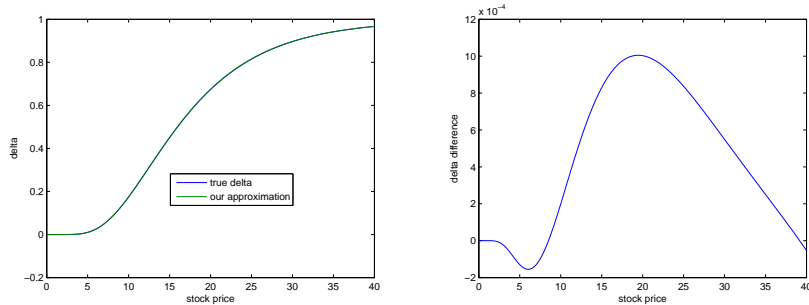


FIGURE 9. Comparison of the delta computed by our bootstrap scheme (2nd order approximation) with the true values under the Black-Scholes model. Model parameters: $t = 0.5, K = 20, \sigma = 0.5, r = 10\%$. Basepoint: $z = x$. The left graph plots the delta computed by our bootstrap method and the true delta. The right graph plots their difference. In our numerical integration, we truncate the half line at 400. Note that in the second figure the scale is 10^{-4} . The x-axis scaled by 10, i.e. the label 400 means the stock price is 40.

butterfly options, where the first derivative of the payoff function has three discontinuities, Figure (8). This oscillation is amplified in the calculation of Greeks. The bootstrap scheme reduces this oscillation dramatically.

For the numerical simulation, we choose the same parameters as those in Section (4.2). The small time step ensures very good error control at each time step. Also, we minimize the truncation error as before by truncating the integral at $x = 400$ and comparing the approximations only on the interval $[0, 40]$ near the strike price $k = 20$. The left graph of Figure (9) plots the true delta and our approximation in the same picture, and the right one plots the difference between these two curves, which shows that the difference between the true value and our approximation is in the order of 10^{-4} with the biggest error around 3.3×10^{-4} . Thus our approximation is quite accurate. For the gamma, we obtain similar results, see Figure 10. The difference is in the order of 10^{-5} , and the biggest error is around 5.6×10^{-5} . In both cases, there are no oscillations on the same scale of the solution.

REFERENCES

- [1] Y. Aït-Sahalia. Closed-form likelihood expansions for multivariate diffusions. *Ann. Statist.*, 36(2):906–937, 2008.
- [2] R. Azencott. Asymptotic small time expansions for densities of diffusion processes. *Lecture Notes Maths*, 1059:402–498, 1984.
- [3] F Black and M. Scholes. The pricing of options and corporate liabilities. *Journal of Political Economy*, 81(3):637–54, May-June 1973.

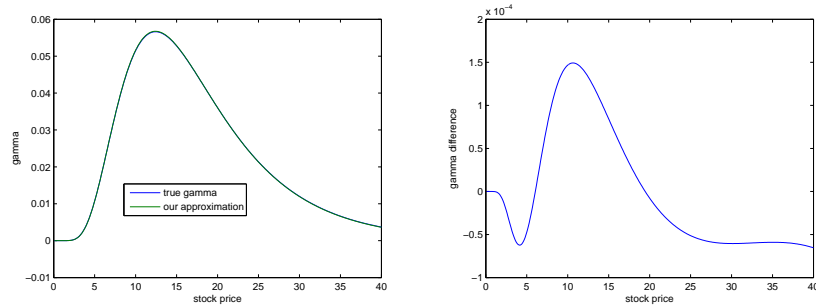


FIGURE 10. Comparison of the gamma computed by our bootstrap scheme(2nd order approximation) with the true values under the Black-Scholes model. Model parameters: $t = 0.5, K = 20, \sigma = 0.5, r = 10\%$. Basepoint: $z = x$. The left graph plots the gamma computed by our bootstrap method and the true gamma. The right graph plots their difference. In our numerical integration, we truncate the half line at 400. Note that in the second figure the scale is 10^{-5} . The x-axis is scaled by 10, i.e. the label 400 means the stock price is 40.

- [4] H. Carmichael. *Statistical methods in quantum optics. 1*. Texts and Monographs in Physics. Springer-Verlag, Berlin, 1999. Master equations and Fokker-Planck equations.
- [5] W. Cheng, R. Costantinescu, N. Costanzino, A. L. Mazzucato, and V. Nistor. Approximate solutions to second order parabolic equations iii: the degenerate case. In preparation.
- [6] W. Cheng, A. L. Mazzucato, and V. Nistor. Approximate solutions to second order parabolic equations ii: time dependent case. Work in progress.
- [7] F. Corielli, P. Foschi, and A. Pascucci. Parametrix approximation of diffusion transition densities. Preprint, 2009.
- [8] R. Costantinescu, N. Costanzino, A. L. Mazzucato, and V. Nistor. Approximate solutions to second order parabolic equations i: analytical estimates. Arxiv Preprint 0910.1562v2, IMA Preprint 2248. Submitted.
- [9] J. Cox. Notes on option pricing 1, constant elasticity of diffusions. unpublished draft, Stanford University, 1975.
- [10] J. Cox and S. Ross. The valuation of options for alternative stochastic processes. *Journal of Financial Economics*, pages 145–166, 1976.
- [11] G. Dorflleitner, P. Schneider, K. Hawlitschek, and A. Buch. Pricing options with green’s functions when volatility, interest rate and barriers depend on time. *Quantitative Finance*, 8(2):119–133, 2008.
- [12] D. Duffie. *Dynamic asset pricing theory*. University Press, 2001.
- [13] D. Emanuel and J. MacBeth. Further results on the constant elasticity of variance call option pricing model. *the Journal of Financial and Quantitative Analysis*, 17(4):533–554, 1982.
- [14] W. Farkas, N. Reich, and C. Schwab. Anisotropic stable Lévy copula processes—analytical and numerical aspects. *Math. Models Methods Appl. Sci.*, 17(9):1405–1443, 2007.

- [15] J.-P. Fouque, G.e Papanicolaou, and R. Sircar. *Derivatives in financial markets with stochastic volatility*. Cambridge University Press, Cambridge, 2000.
- [16] C. Gardiner. *Handbook of stochastic methods for physics, chemistry and the natural sciences*, volume 13 of *Springer Series in Synergetics*. Springer-Verlag, Berlin, third edition, 2004.
- [17] J. Gatheral. *The volatility surface: a practitioner's guide*. John Wiley and Sons, 2006.
- [18] P. Greiner. An asymptotic expansion for the heat equation. *Arch. Rational Mech. Anal.*, 41:163–218, 1971.
- [19] P. Hagan and D. Woodward. Equivalent black volatilities. *Applied Mathematical Finance*, 6(3):147 – 157, 1999.
- [20] E. Hsu. *Stochastic analysis on manifolds*, volume 38 of *Graduate Studies in Mathematics*. American Mathematical Society, Providence, RI, 2002.
- [21] J. Hull. *Options, Futures and Other Derivatives*. Prentice Hall, 2007. Sixth edition.
- [22] J. Kampen. The wkb-expansion of the fundamental solution of linear parabolic equations and its applications. Submitted.
- [23] C. Lo, P. Yuen, and C. Hui. Constant elasticity of variance option pricing model with time-dependent parameters. *Int. J. Theor. Appl. Finance*, 3(4):661–674, 2000.
- [24] A Lunardi. *Analytic semigroups and optimal regularity in parabolic problems*. Progress in Nonlinear Differential Equations and their Applications, 16. Birkhäuser Verlag, Basel, 1995.
- [25] H. McKean, Jr. and I. Singer. Curvature and the eigenvalues of the Laplacian. *J. Differential Geometry*, 1(1):43–69, 1967.
- [26] R. Melrose. *The Atiyah-Patodi-Singer index theorem*, volume 4 of *Research Notes in Mathematics*. A K Peters Ltd., Wellesley, MA, 1993.
- [27] R. Merton. Theory of rational option pricing. *Bell Journal of Economics*, 4(1):141–183, Spring 1973.
- [28] S. Minakshisundaram and A. Pleijel. Some properties of the eigenfunctions of the Laplace-operator on Riemannian manifolds. *Canadian J. Math.*, 1:242–256, 1949.
- [29] A. Pazy. *Semigroups of linear operators and applications to partial differential equations*, volume 44 of *Applied Mathematical Sciences*. Springer-Verlag, New York, 1983.
- [30] H. Risken. *The Fokker-Planck equation*, volume 18 of *Springer Series in Synergetics*. Springer-Verlag, Berlin, second edition, 1989. Methods of solution and applications.
- [31] M. Schroder. Computing the constant elasticity of variance option pricing formula. *the Journal of Finance*, 44(1):211–219, 1989.
- [32] S. Shreve. *Stochastic calculus for finance. II*. Springer Finance. Springer-Verlag, New York, 2004. Continuous-time models.
- [33] M. Taylor. *Pseudodifferential operators*, volume 34 of *Princeton Mathematical Series*. Princeton University Press, Princeton, N.J., 1981.
- [34] M. Taylor. *Partial differential equations. I*, volume 115 of *Applied Mathematical Sciences*. Springer-Verlag, New York, 1996. Basic theory.
- [35] S. Varadhan. Diffusion processes in a small time interval. *Comm. Pure Appl. Math.*, 20:659–685, 1967.
- [36] D. Vassilevich. Heat kernel expansion: user's manual. *Phys. Rep.*, 388(5-6):279–360, 2003.

E-mail address: cheng@math.psu.edu

DEPARTMENT OF MATHEMATICS, PENNSYLVANIA STATE UNIVERSITY, UNIVERSITY PARK, PA 16802

E-mail address: costanzi@math.psu.edu

DEPARTMENT OF MATHEMATICS, PENNSYLVANIA STATE UNIVERSITY, UNIVERSITY PARK,
PA 16802

E-mail address: `jcl12@psu.edu`

DEPARTMENT OF MARKETING, SMEAL COLLEGE OF BUSINESS, AND DEPARTMENT OF
STATISTICS, PENNSYLVANIA STATE UNIVERSITY, UNIVERSITY PARK, PA 16802

E-mail address: `mazzucat@math.psu.edu`

DEPARTMENT OF MATHEMATICS, PENNSYLVANIA STATE UNIVERSITY, UNIVERSITY PARK,
PA 16802

E-mail address: `nistor@math.psu.edu`

DEPARTMENT OF MATHEMATICS, PENNSYLVANIA STATE UNIVERSITY, UNIVERSITY PARK,
PA 16802